

A finite-discrete element approach for modelling polyethylene pipes subjected to axial ground movement

Masood Meidani , Mohamed A. Meguid & Luc E. Chouinard

To cite this article: Masood Meidani , Mohamed A. Meguid & Luc E. Chouinard (2020) A finite-discrete element approach for modelling polyethylene pipes subjected to axial ground movement, International Journal of Geotechnical Engineering, 14:7, 717-729, DOI: [10.1080/19386362.2018.1483812](https://doi.org/10.1080/19386362.2018.1483812)

To link to this article: <https://doi.org/10.1080/19386362.2018.1483812>

 Published online: 03 Jul 2018.

 Submit your article to this journal [↗](#)

 Article views: 102

 View related articles [↗](#)

 View Crossmark data [↗](#)

 Citing articles: 1 View citing articles [↗](#)

RESEARCH ARTICLE



A finite-discrete element approach for modelling polyethylene pipes subjected to axial ground movement

Masood Meidani, Mohamed A. Meguid  and Luc E. Chouinard

Civil Engineering and Applied Mechanics, McGill University, Montreal, Quebec, Canada

ABSTRACT

The response of medium-density polyethylene (MDPE) pipes subjected to ground movement is often investigated using soil-pipe interaction models that were originally developed for steel pipes. In this study, the behaviour of MDPE pipes buried in dense sand under pull-out force is investigated using a coupled finite-discrete element framework. The pipe is modelled using finite elements whereas the granular soil is modelled using discrete elements. The model is validated using experimental data and then used to investigate the response of the pipe and the surrounding soil. The response of the MDPE pipe-soil system to axial loading is found to differ significantly from that of steel pipes due to the elongation and distortion that develop in the MDPE pipes, which affect the mobilized friction forces along the pipe. This study demonstrates that caution must be exercised when using current methods in the analysis of MDPE pipes.

ARTICLE HISTORY

Received 14 April 2018
Accepted 30 May 2018

KEYWORDS

Soil-pipe interaction; finite-discrete element; polyethylene pipes; axial ground movement

1. Introduction

Buried pipelines are used worldwide to transport natural resources such as water, oil and gas. These critical infrastructures are considered to be lifelines for modern cities and failure of these pipes can have significant impact on the economy and the environment. Some of the common causes of failure are generally related to the deterioration of the pipe material or the surrounding backfill soil. However, natural hazards such as permanent ground deformation (PGD) caused by earthquakes can have damaging effects on pipelines. The ninth report of the European Gas Pipeline Incident Date Group (European Gas Pipeline Incident Data Group 2015) presented a distribution of failure incidents that happened from 2004 to 2013. It was concluded that about 16% of pipeline incidents happened due to ground movement which rank third among major causes of incidents.

Since the early 1960s, researchers have studied soil-pipe interaction to understand the behaviour of buried pipelines subject to permanent ground movements. These studies include field tests, full scale laboratory experiments and centrifuge models (e.g. Trautmann and O'Rourke 1983; Rizkalla, Simmonds, and Uptirove 1991; Konuk et al. 1999; Phillips, Nobahar, and Zhou 2004; Weerasekara and Wijewickreme 2008; Daiyan and Kenny, 2011; Mohamedzein et al. 2016; Joshaghani, Raheem, and Mousavi 2016; Robert et al. 2016; Ono et al. 2018). For example, Daiyan and Kenny (2011) performed a set of centrifuge tests on rigid pipes buried in dense sand to determine the axial-lateral interaction of the soil-pipe system; Bilgin, Stewart, and O'Rourke (2007) conducted two field pull-out tests on cast iron pipes buried in dense and loose sands to determine the impact of thermal variation on the pipe response to different loading conditions.

In addition to the experimental studies, numerical and analytical investigations have been performed to determine the response of buried pipes subjected to either lateral or axial ground movements (e.g. Cocchetti et al. 2009; Rahman and Taniyama 2015; Roy et al. 2016; Almahakeri, Moore, and Fam 2016; Zhang, Liang, and Han 2016; Meidani, Meguid, and Chouinard 2017). Most of these studies used the finite element method (FEM) to model both the pipelines and the surrounding soil. Guo and Stolle (2005) carried out a numerical investigation using ABAQUS software to explain the range of lateral soil resistance obtained by different researchers. The effects of burial depth, overburden ratio, soil dilatancy and strain hardening were investigated. Kunert, Otegui, and Marquez (2012) proposed a nonlinear finite element technique to assess the behaviour of pipelines buried in rain-forest regions, which are prone to failures by axial stresses from land movement. Recently, Naeini et al. (2016) developed a finite element model to investigate the response of buried HDPE pipeline to fault movements. The numerical results agreed with experimental data and, therefore, it was concluded that the FEM method is suitable for analyzing this class of problems. One of the reported challenges was related to modelling the soil-pipe interaction under large deformation and understanding particle movements in the close vicinity of the pipe.

An alternative approach to analyze this class of problems and capture the soil behaviour around the pipe is using the discrete element method (DEM). This approach has been used by researchers to investigate different soil-structure interaction problems (e.g. Cui and O'Sullivan 2006; Chen et al. 2012; Tran and Meguid 2014; Ahmed, Tran, and Meguid 2015). Meidani, Meguid, and Chouinard (2017) conducted 3D discrete element analysis

of a steel pipe buried in granular material to investigate the response of the pipe under relative ground movement. Using the DEM, particle movements around the pipe and the changes in radial stresses were evaluated with a reasonable accuracy. The rigid steel pipe was modelled using facet discrete elements that do not allow for the development of axial or radial deformation in the pipe structure. Although this is suitable for rigid pipes, flexible polyethylene pipes (PE) may undergo both axial and radial deformation under axial loading and therefore, the pipe response and the associated interaction with the surrounding soil may not be accurately modelled using discrete elements.

To take advantage of both the finite and discrete element methods, coupling the two approaches has provided researchers with the flexibility of solving a wide range of geotechnical engineering problems involving buried structures. Structural elements are usually modelled using finite elements whereas the surrounding soil particles are modelled using discrete elements. Several algorithms have been developed to facilitate the load transfer between the two domains. A procedure for combining finite and discrete elements is to simulate the shot peening process was proposed by Han, Owen, and Peric (2002). Fakhimi (2009) developed an algorithm for coupling the finite and discrete element methods and used the coupled model to simulate the deformable membrane and the encased soil samples in laboratory triaxial tests. The membrane was modelled using finite elements (FE) while the soil was modelled using discrete elements (DE). Villard et al. (2009) proposed a coupled FE-DE approach to model earth structures reinforced by geosynthetic material. The framework was used to model the interaction between a geosynthetic sheet and the surrounding soil. Dang and Meguid (2013) proposed a coupled FE-DE approach to model soil-structure interaction problems involving large deformations. Interface elements were introduced at the boundary between the two domains to transmit the interaction forces between the finite and discrete elements. Tran, Meguid, and Chouinard (2013) proposed a similar finite-discrete element framework for the 3D modelling of geogrid-soil interaction under pull-out loading condition.

In this study, a coupled FE-DE approach is developed and used to investigate the response of MDPE pipe buried in dense sand and subjected to axial soil movements. A numerical model that is able to capture the response of both the pipe and backfill material is created. Microstructure parameters needed for the discrete element analysis are determined using triaxial test data and the overall model performance is validated using analytical solutions. The validated model is then used to determine the response of the pipe and the backfill material. The numerical results are also compared with experimental data. Using the developed approach, the detailed behaviour of the soil surrounding the pipeline is investigated and the stresses developing in the pipe structure are evaluated. Finally, current guidelines for estimating soil loads on flexible pipes subjected to relative axial displacement are reviewed on the basis of the numerical results

2. Coupled finite-discrete element framework

The coupled 3D Finite-Discrete element algorithm used for this study was originally developed by Dang and Meguid (2010), Dang and Meguid (2013) and Tran, Meguid, and Chouinard (2013) to model the interaction between the finite and discrete element domains. The developed approach was implemented into *YADE*, an open source code for DE analysis (Kozichi and Donze, 2008; Smilauer et al., 2010) and is briefly discussed in the following sections.

2.1. The discrete elements

The DEM is a numerical technique that models the interaction between individual particles as they come in contact with different boundaries. The discrete particles interact with each other at their contact points in a dynamic process that reaches static equilibrium when the internal forces are balanced. The dynamic behaviour is represented numerically by a time stepping algorithm with an explicit finite difference scheme.

The contact laws between two particles 1 and 2 of radii r_1 and r_2 used in this study are summarized as follows:

$$\Delta = r_1 + r_2 - d_0 \quad (1)$$

where d_0 is the distance between two centres. The interaction force between two contacting particles is represented by a force vector F . The force vector can be decomposed into normal (F_N) and tangential forces (δF_T) which are calculated using the normal (K_N) and the tangential (K_T) stiffnesses at the contact point as expressed as follows.

$$F_N = K_N \cdot \Delta_N \text{ and } \delta F_T = -K_T \cdot \delta \Delta_T \quad (2)$$

where Δ_N and $\delta \Delta_T$ are the normal and incremental tangential amounts of overlap between the two particles. Particles normal stiffness (K_N^1 and K_N^2) are used to calculate the normal stiffness of the contact between two particles:

$$K_N = \frac{K_N^1 \cdot K_N^2}{K_N^1 + K_N^2} \quad (3)$$

The particles normal stiffness are calculated using the particle material modulus E_i and radius r such that

$$K_N^1 = 2E_1r_1 \text{ and } K_N^2 = 2E_2r_2 \quad (4)$$

A portion of the contact normal stiffness is used to calculate the tangential stiffness, $K_T = \alpha K_N$. There is no limit for the normal force at the contact; however, the limiting value for the tangential force F_T is defined as

$$F_T = \frac{F_T}{F_N} F_N \tan_{\text{micro}} \text{ If } F_T \gg F_N \tan_{\text{micro}} \quad (5)$$

where micro is the micro friction angle between two particles.

The contact law is capable of transmitting moments between particles. The angular rotation vector θ_r is employed to determine the rotational resistance between the two particles. This value is calculated by adding the incremental angular rotations as follows (Smilauer et al. 2010):

$$\theta_r = \sum d\theta_r \quad (6)$$

The rotational stiffness of the contact (K_r) is used to calculate the resisting moment M_r at the contact. A limiting value of the moment is described in terms of the normal force vector and a dimensionless coefficient (η_r) such that:

$$M_r = K_r \cdot \theta_r, \quad M_{r\text{lim}} = \eta_r F_N \left(\frac{r_1 + r_2}{2} \right) \quad (7)$$

$$K_r = \beta_r \cdot \left(\frac{r_1 + r_2}{2} \right)^2 \cdot K_T \quad (8)$$

where β_r is the rolling resistance coefficient.

2.2. The finite elements

The dynamic relaxation method is used in developing the coupled framework including both the finite and discrete element domains. The general equation of the FE approach is

$$Kx + cM\dot{x} + M\ddot{x} = P \quad (9)$$

Where P the external force is vector; x is the displacement vector; M is the mass matrix; c is the damping coefficient and K represents the stiffness matrix.

The maximum time step $[\Delta_{\text{FE}}]$ that meets the convergence condition of the system is determined based on the maximum eigenvalue (λ_m) which is calculated using the element consistent tangent stiffness:

$$[\Delta_{\text{FE}}] = \frac{2}{\sqrt{\lambda_m}} \quad (10)$$

$$\lambda_m \leq \max_i \sum_{j=1}^n \frac{|K_{ij}|}{M_{ij}} \quad (11)$$

where M_{ij} is an element in the diagonal mass matrix; and K_{ij} is an element in the global tangent stiffness matrix.

2.3. Interface elements

Interface elements are employed in the coupled framework to transfer the contact forces between the FE and DE domains. These elements are generated such that they follow the finite element nodes. Since hexahedral elements are used for the FE domain, the contact surface between the two domains is divided into four interface elements by adding a temporary node at the centre of each finite element as expressed as follows.

$$X^{(0)} = \frac{1}{4} \sum_{i=1}^4 X^{(i)} \quad (12)$$

where $X^{(i)}$ is the coordinate of node i of the quadrilateral element. Figure 1 shows a schematic of the interaction between discrete particles, interface and finite elements. The contact law between the interface and discrete elements is the same as that used for particle–particle interaction. Following the contact between a DE particle and an interface element, the normal and tangential interaction forces are calculated using the normal overlap and incremental tangential displacement of the contact. The total contact force is determined

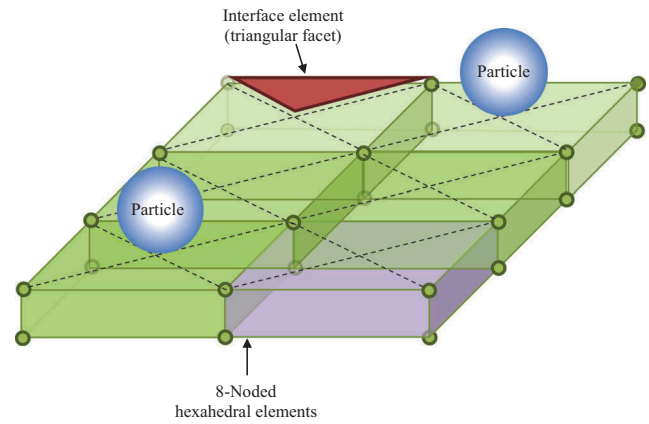


Figure 1. A schematic of the coupling between finite and discrete elements using interface elements.

by summing the normal and tangential force vectors ($\bar{F}_N + \bar{F}_T$). Eq. 13 is used to compute the transmitted forces to the FE nodes using the interaction forces.

$$\bar{F}_i + \bar{F}_{\text{contact}} \cdot N_i = \bar{F}_N + \bar{F}_T \cdot N_i \quad (13)$$

where N_i is the shape function calculated using the natural coordinates of the contact point.

A typical FE-DE computational cycle was discussed and reported by Dang and Meguid (2010); Dang and Meguid (2013)).

3. Modeling pipe-soil interaction

Previous studies on pipeline resistance to axial soil movements have been mainly focusing on steel pipes and only a few studies addressed PE pipes (e.g. Anderson 2004; Weerasekara 2007). Design guidelines (e.g. ASCE 1984; ALA 2001) are based on results obtained using steel pipes and their application to PE pipes may not be appropriate given the viscoelastic nature and the relatively low stiffness of the PE material. In addition, Karimian (2006) and Meidani, Meguid, and Chouinard (2017) reported that the available guidelines may underestimate the axial soil pressure acting on pipes installed in cohesionless soil, particularly for dense soil.

3.1. Model generation

The FE-DE model used in this study is created based on the experimental work reported by Weerasekara (2007). The experiments comprised an MDPE pipe with outside diameter of 114 mm buried in a soil chamber 3.8 m in length, 2.5 m in width and 1.3 m in height. The pipe was installed at a depth of 0.6 m below the surface. Dense Fraser River sand with relative density of 75% was used in the experiment. The grain size distribution of the sand material is shown in Figure 2 and the relevant properties are summarized in Table 1. The rigid box hosting the soil and the pipe was reinforced with steel frames to prevent lateral deformation and the inner surface was designed to ensure minimum friction between the soil and the walls of the chamber. The pipe was pulled out

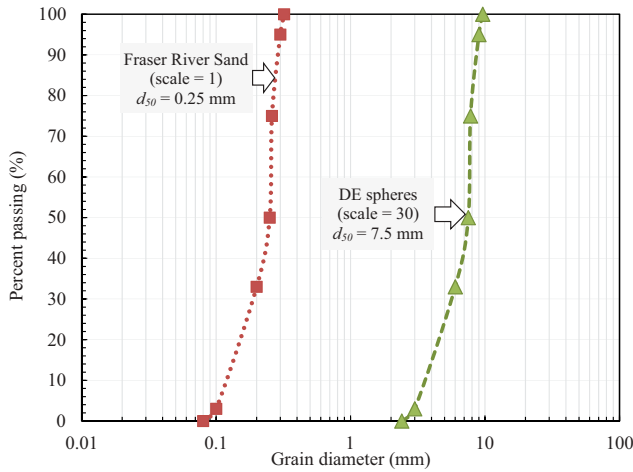


Figure 2. Particle size distributions for the Fraser River Sand and the generated DE particles.

Table 1. Soil properties of backfill material (Fraser River Sand).

Parameter	Value
Specific gravity	2.72
Young's modulus, E_i (MPa)	40
Unit weight (kN/m^3) – (75% relative density)	16
Internal friction angle θ (Degree)	45
Cohesion (kN/m^2)	0
Poisson ratio, ν	0.3
Porosity, n	0.41

incrementally from the backfill following a displacement-controlled loading condition and the reaction force was continuously measured.

The numerical analysis is conducted using a modified version of the open source code *YADE* (Kozicki and Donzé 2008; Šmilauer et al. 2010). The soil particles are modelled using discrete elements while the pipeline is modelled using finite elements. Interface elements are employed to model the interaction between these two domains as discussed in Section 2. The MDPE pipeline is modelled using eight-noded hexahedral elements. The modelled pipe has 114.3 mm outside diameter and 10.3 mm wall thickness. The results of the laboratory experiments performed on the MDPE pipe based on uniaxial compression (Anderson 2004) and pull-out (tensile) test data (Weerasekara 2007) are presented in Figure 3a. The response is characterized by slight nonlinear response up to 3% strain. Konder (1963) proposed a hyperbolic stress-strain relationship for PE pipes as follows:

$$\sigma = E_i \left(\frac{\varepsilon}{1 + \eta\varepsilon} \right) \quad (14)$$

where ε is the strain, E_i is the initial Young's modulus, σ is the stress and η is a constant. The hyperbolic relationship for the investigated PE pipe is superimposed on the experimental data in Figure 3a. The relationship was found to represent the pipe response and agree well with the experimental data. Given the small strain level expected in the pull-out experiments, the hyperbolic model was used to determine an approximate linear elastic model that represents the pipe response as shown in Figure 3b. At strain level of up to 5%, the modulus of elasticity E_i was found to be approximately 550 MPa.

The 3.85 m long MDPE pipe was modelled using 1232 solid elements that measure 5 cm \times 2.25 cm each overlain by 4928 interface elements. Details of the different components of the finite element model used to represent the pipe are shown in Figure 4.

Particle up-scaling is used to keep the number of particles within a feasible range for the DEM. Ding et al. (2014) conducted a 3D numerical study on the effect of particle up-scaling on the macroscopic response of discrete element samples. It was found that the ratio between the smallest sample lengths (L) to the median of the particle diameters (d) should be kept below 30 to minimize the effects of particle up-scaling. Given the size of the test chamber and the pipe diameter in this study, d_{50} of 7.5 mm is selected for the discrete elements, which results in 4,900,000 particles. The corresponding scaled particles size distribution is shown in Figure 2.

To keep the problem size manageable and further reduce the number of particles, a parametric study was performed to determine the minimum width (Y) and the height (Z) of the model that does not affect the pipe response, while preserving the full length (X) of the pipe (see Figure 5a). The results of the parametric study are presented in Figures 5b and c for the model width and height, respectively. Figure 5b shows the change in the pull-out force as the model width increases from 0.3 m to 2.75 m for applied displacement of 15 mm. The pull-out force was found to rapidly decrease as the model width (Y) increased and reached a plateau at a model width of about 0.5 m. This means that increasing the model width beyond 0.5 m does not have a significant impact on the pull-out response of the pipe. Similarly, Figure 5c shows that the pipe response reached a plateau at $Z/2$ of 0.25 m which corresponds to a model height 0.5 m. These model dimensions were, therefore, adopted in the numerical analysis presented in this study. The overlying backfill material above 0.5 m was replaced using equivalent surcharge pressure that is uniformly distributed at the model surface.

To generate the discrete element particles, the radius expansion method is used in combination with the particle size distribution shown in Figure 2. A cloud of non-contacting particles is first created, then the particles located within the pipe circumference are removed and the radius of the spheres are increased to achieve the target porosity of 0.41, which corresponds to that used in the experiment. The set of particles is allowed to move under gravity and the assembly is then cycled until equilibrium condition is reached. The final three-dimensional model includes a total of 345,000 spherical particles as depicted in Figure 6a. To illustrate the particle distribution in the close vicinity of the pipe, a front view of the model (in the Y - Z plane) is shown in Figure 6b.

3.2. Model calibration

Input parameters used in the discrete element analysis include two major groups: (i) physical parameters (friction angle, cohesion and Young's modulus), and (ii) dimensionless coefficients (rolling and shear stiffness coefficients, maximum resistant moment factor, etc.). A calibration procedure is needed to determine these parameters for a given soil condition. The model used in this study was calibrated by

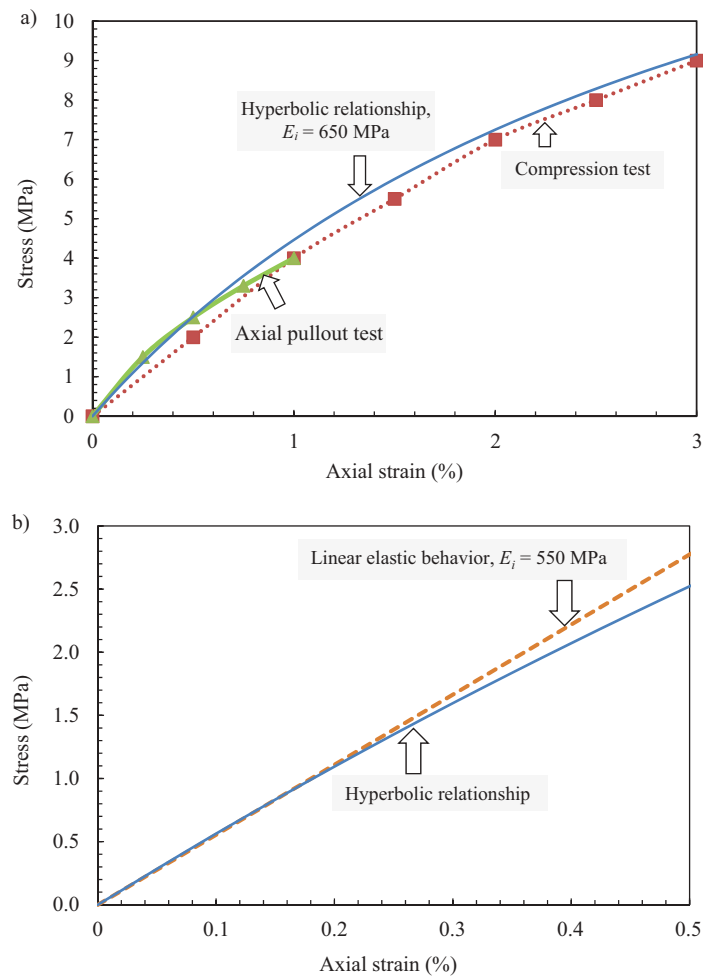


Figure 3. (a) Stress-strain response of the MDPE pipe from compression test, axial pull-out test and the hyperbolic model; (b) comparison between linear elastic and the hyperbolic model.

simulating triaxial tests conducted on Fraser River sand (Karimian 2006) and comparing the calculated response with the measured values. Table 1 presents the mechanical properties of the Fraser River Sand based on triaxial tests performed at 25 kPa confining pressure. Model calibration details have been reported elsewhere (Meidani, Meguid, and Chouinard 2017) and only a summary of the obtained parameters that are needed for the discrete element analysis is provided in Table 2.

3.3. Validation of the numerical model

After creating both the discrete element assembly and the finite element model of the pipe, the coupled model is allowed to freely settle under gravity using the input parameters presented in Table 2. No friction was considered between the rigid walls and the contained particles to properly simulate the test conditions. A vertical pressure equal to 5.6 kPa was then applied over the coupled model to represent the removed soil layer ($\gamma = 16$ kN/m³). The contact pressure distribution acting on the pipe is first calculated at selected locations along the pipe circumference using the developed model and the results are compared with Hoeg's analytical solution (Hoeg, 1986). The numerical calculation was

performed at several zones along the pipe to ensure that the model provides consistent results everywhere in the model. The investigated zones (shown in Figure 7) include: (1) from $X = 0.5$ m to 1 m; (2) from $X = 1.75$ m to 2.25 m; (3) from $X = 3$ m to 3.5 m. The average soil pressure acting on the pipe using the analytical solution and the numerical model are compared for each zone (Figure 7a and Table 3). The calculated pressure at the crown of the pipe for the three examined zones (1, 2 and 3 in Figure 7b) was found to be 6.22, 6.01 and 5.98 kPa, respectively. These values are consistent with the analytical solution that predicted a pressure of 5.24 kPa at the same location. Based on the results presented in Table 3, the maximum difference between the average pressure calculated at the three zones and the 2D analytical solution was found to be $\pm 15\%$. This level of accuracy is considered acceptable given the 3D nature of the problem and the approximations made in developing the numerical model.

After the initial conditions are verified, the pull-out test is performed using a displacement control approach. The vertical pressure acting on the model is kept constant throughout the analysis at $\sigma_v = 5.6$ kPa using the method developed by Tran, Meguid, and Chouinard (2013). The stiffness of the interface is set equal to that of the discrete particles and the interface friction angle is determined by matching the

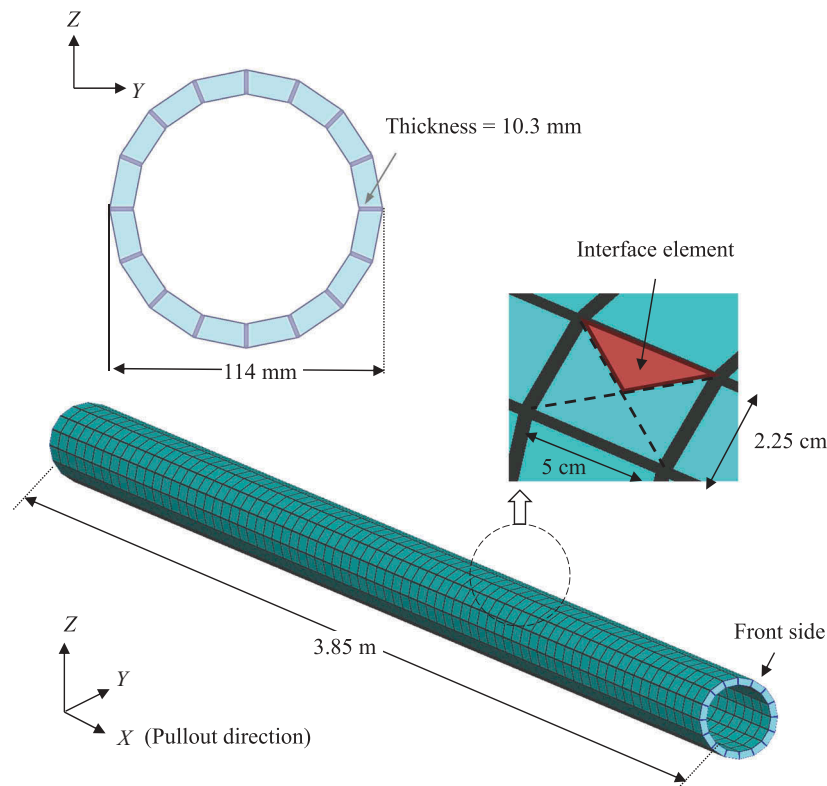


Figure 4. The finite element mesh and interface elements used to model the MDPE pipe.

experimental results. This approach is consistent with that reported by Tran, Meguid, and Chouinard (2013) and Villard et al. (2009). The pull-out force is incrementally applied to the pipe and the corresponding displacements at the leading end are presented in Figure 8. The pull-out force increased non-linearly with the initial increase in displacement. The maximum pull-out force reached about 6.4 kN at applied displacement of 14 mm. The measured response is superimposed on the numerically calculated results as shown in Figure 8. Close agreement was found between the experimental and numerical responses with a maximum difference in pull-out force of about 9% with a maximum measured value of 6.8 kN.

In addition to the model validation using the mobilized soil resistance to pull-out loading, the changes in axial strains (ϵ_x) developing at the leading end of the pipe are also calculated for different pull-out forces and the results are compared with the measured values as shown in Figure 9. The relationship is almost linear for the range of strains experienced by the pipe during the pull-out process. The axial strain calculated at the maximum pull-out force is found to be $3740 \mu\epsilon$. This is consistent with the experimental results reported by Weerasekara (2007) where the maximum measured strain was found to be $3800 \mu\epsilon$. The corresponding displacements at the leading end are also examined in Figure 10. The maximum displacement obtained using the numerical model is about 14 mm whereas the measured value is about 12 mm. However, the overall relationship is properly captured using the developed model experimental results are respectively 14 mm and 12 mm (Figure 10). These results validate the

adequacy of the developed model in representing the soil-pipe interaction under axial loading conditions.

4. Results and discussions

The detailed response of the pipe and the surrounding soil are investigated in this section. This includes the strains and displacements developing along the pipe in the longitudinal and transverse directions. The accuracy of the available closed form solution in predicting the maximum pull-out force is then evaluated. To take advantage of the coupled model, the changes in contact force distribution and the displacement field around the pipe is also examined.

4.1. Response of the pipe

The distributions of horizontal displacements developing along the pipe for different pull-out displacements (U_x) are presented in Figure 11a. The pipe displacements are found to be generally non-uniform with most of the movements occur near the leading end of the pipe (length = 3.8 m). Small displacements were calculated within half of the pipe length located in the opposite side of the applied load. The contours of horizontal displacement in the pipe structure at applied displacement of 14 mm are illustrated in Figure 11b. The figure shows the concentration of displacements developing in the pipe.

To understand the displacement pattern presented in Figure 11 the investigated PE pipes, it is worthwhile comparing the response with that reported for rigid pipes. Pull-out

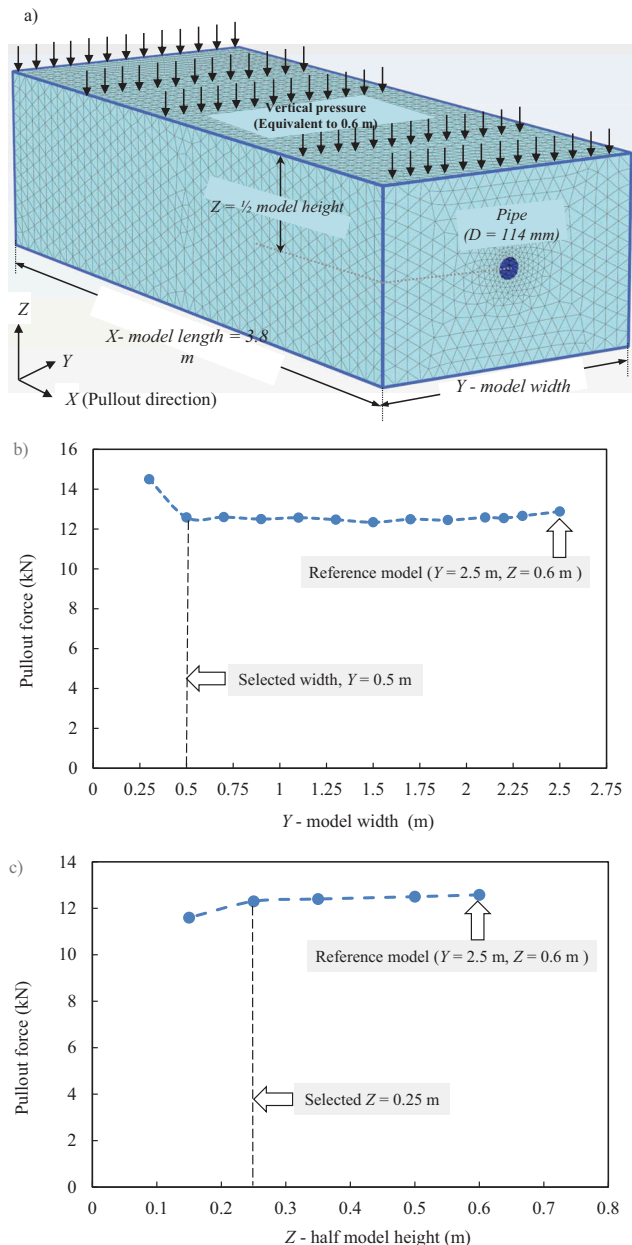


Figure 5. (a) Finite element model used to examine the effect of model dimensions; (b) the effect of model width on pull-out force; (c) the effect of model height on pull-out force.

experiments performed on rigid steel pipes (Karimian 2006) revealed that entire length of the pipe starts to move immediately after applying the axial force indicating that the friction between the soil particles and the pipe is mobilized over the entire length of the pipe. This is attributed to the difference in stiffness between the rigid pipe and the surrounding soil. Hence, the pull-out test of a rigid pipe can be assumed as an ‘element’ test, and the frictional resistance can be considered uniform along the entire length of the pipe. On the other hand, for MDPE pipe a small section of the pipe experiences slipping at the beginning of the test. With the increase in loading, the slipping section propagates along the pipe. Hence, the frictional resistance along the MDPE pipe is not uniform and the maximum pull-out force is reached when the entire length of the pipe starts to move. It is also noted that

MDPE pipes are more extensible than rigid steel pipes, and therefore both elongation and reduction in cross-section may develop during the pull-out process. It can, therefore, be concluded that the axial soil resistance in this case is a function of the pipe length and the force-displacement results are valid as long as the pipe does not completely slip out of the soil.

The evolution of the axial strains (ϵ_x) along the length of the pipe is presented in Figure 12a for different leading-end displacements (U_x). The distribution of strains is found to be consistent with the displacement patterns presented in Figure 11 as well as the results reported by Weerasekara (2007). Figure 12b shows the contours of the axial strains at applied leading-end displacement of 14 mm . It can be seen that at this displacement level, the axial strain at front edge of the pipe is about $3300 \mu\epsilon$ whereas at the middle of the pipe the calculated strain is found to be about $1000 \mu\epsilon$ which is approximately 3 times smaller in magnitude compared to the strain found at front of the pipe. This confirms the non-uniform nature of the frictional resistance mobilized on the pipe surface resulting from the non-uniform elongation developing in the pipe.

To investigate the distortion that develops in the pipe cross-section during the pull-out process, the displacements in the transverse (Y) direction are presented in Figure 13a at four selected locations on the pipe circumference. The maximum deformation in the Y direction was found to develop at the springline in the positive Y direction with no significant displacement calculated at the crown. This reveals that the circular shape of the pipe experiences slight distortion during the pull-out process. This can be illustrated by the displacement contours presented in Figure 13b. The three-dimensional distribution of displacement along the pipe length at applied displacement of 14 mm indicates that the distortion of the pipe cross-section is more pronounced near the front side of the pipe.

4.2. Pull-out resistance

The pull-out force (F_A) per pipe unit length according to ASCE (1984) guidelines is expressed by,

$$F_A = \gamma' \times H \times (\pi D L) \times \left(\frac{1 + K_0}{2} \right) \times \tan(\delta) \quad (15)$$

Where γ is soil density; H is the burial depth; D is the pipe diameter; L is the pipe length; K_0 is the coefficient of lateral earth pressure and δ is the interface friction angle between pipe. For the test sample, the resulting pull-out force is 1.13 kN/m .

The relationship between the pipe displacement (U_x) at the leading-end and the corresponding pull-out force per unit length of the pipe is presented in Figure 14. The numerical analysis showed a maximum of pull-out force of 1.68 kN/m . Compared with the closed-form solution, it can be seen that the current guideline underestimates the maximum unit pull-out force for PE pipes. Another limitation of Eq. [15] is the related to assumptions of the soil state around the pipe during axial ground movements. In deriving this expression, the soil

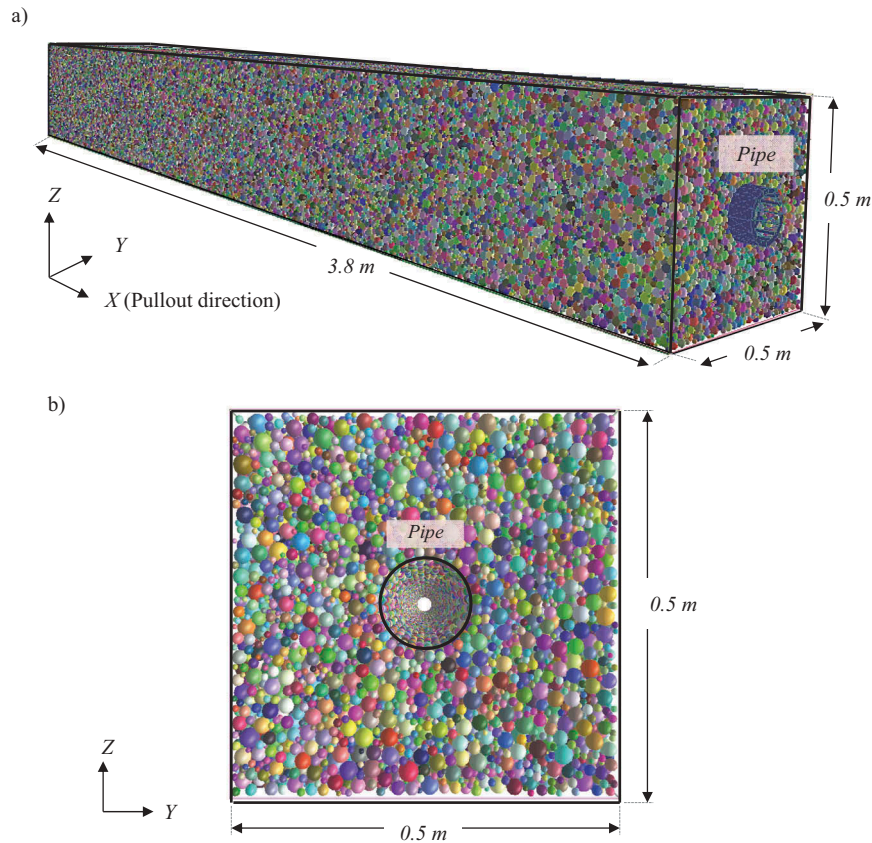


Figure 6. (a) Three-dimensional view of the model showing the pipe and the surrounding particles; (b) front view of the model.

Table 2. Input parameters used in the coupled FE-DE analysis.

Type of element	Parameter	Value
Discrete particle	Density (kg/m^3)	2720
	Particle modulus, E (MPa)	150
	Ratio K_T/K_N , α	0.7
	Micro friction angle, μ_{micro} (Degree)	45
	Rolling resistance coefficient (β_r)	0.15
	η_r	1
Finite element	Damping ratio	0.2
	Young's modulus, E (MPa)	550
Interface element	Poisson's ratio	0.46
	Material modulus, E (MPa)	150
	Ratio K_T/K_N , α	0.7
	Micro friction angle, μ_{micro} (Degree)	40

was assumed to remain at-rest condition. However, Meidani, Meguid, and Chouinard (2017) showed that this assumption may not be valid when the pipe is buried in dense granular soil as the earth pressure condition becomes somewhere between passive and at-rest modes which significantly changes the value of K_0 in Eq. [15].

4.3. Soil response to pipe movement

Figure 15 shows the displacement field within the soil domain in the vicinity of the pipe when the leading end displacement reaches 14 mm. Most of the soil movement was found to occur near the front face of the box where the pipe experiences the

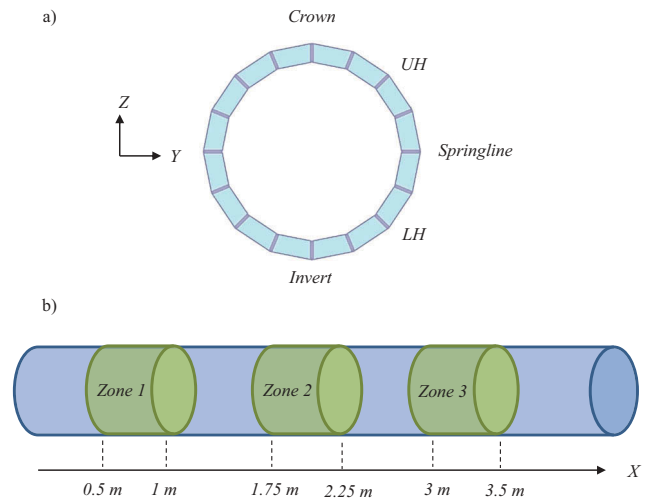


Figure 7. (a) Investigated locations on the pipe circumference; (b) zones used for the initial stress calculation.

Table 3. Comparison between the numerical results and the analytical solution of initial pressure distribution (kPa) around the pipe.

Location	Hoeg (1968)	Zone 1	Zone 2	Zone 3
Crown	5.24	6.22	6.01	5.98
UH	7.70	8.95	7.94	8.29
Springline	10.16	11.34	11.82	10.78
LH	7.70	6.89	6.63	7.24
Invert	5.24	4.87	4.45	4.51

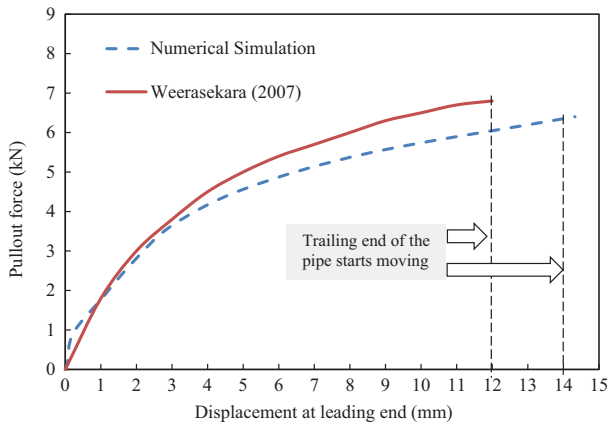


Figure 8. Comparison between the calculated and measured pull-out responses of the pipe.

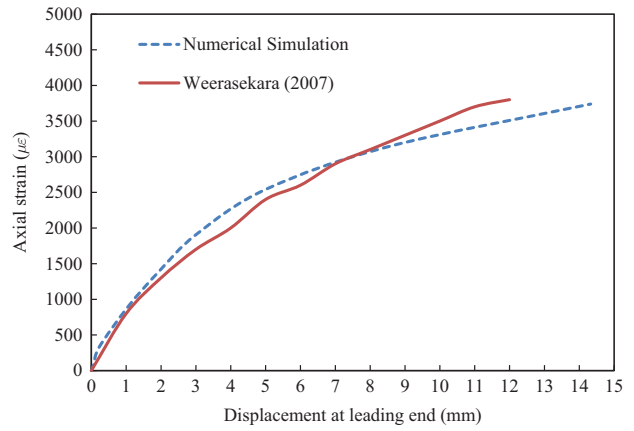


Figure 10. Relationship between strains and displacements developing at the leading-end of the pipe.

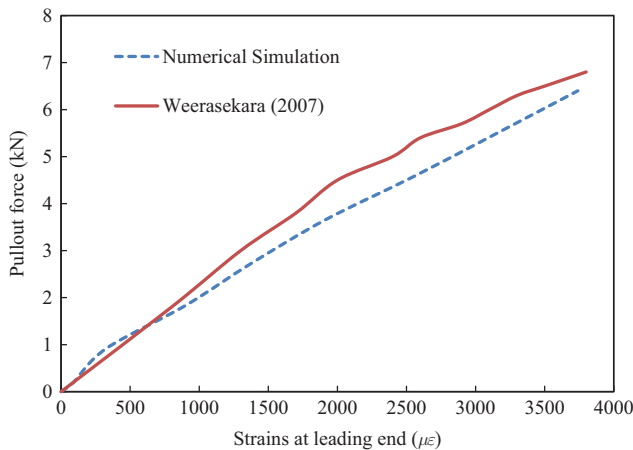


Figure 9. Relationship between the pull-out force and the strains developing at the leading-end of the pipe.

most elongation. No significant particle movement was recorded near the end of the pipe. Particle movements were characterized by a horizontal pattern that gradually changed to point upward near the front side of the box. It was also found that particle displacements are more significant above the pipe where no wall or rigid boundary exists as compared to the lower boundary below the pipe. The particle movement pattern is in general agreement with the pipe elongation and shows the effect of pipe stiffness on the response of the surrounding soil.

Figure 16 shows the contact force network developing within the soil domain for two different loading stages: (a) initial condition and (b) at applied displacement of 14 mm. Each contact force is represented by a line such that the line width is proportional to the magnitude of the contact force. Before the pull-out force is applied (Figure 16a), the contact forces are found to be relatively homogeneous around the

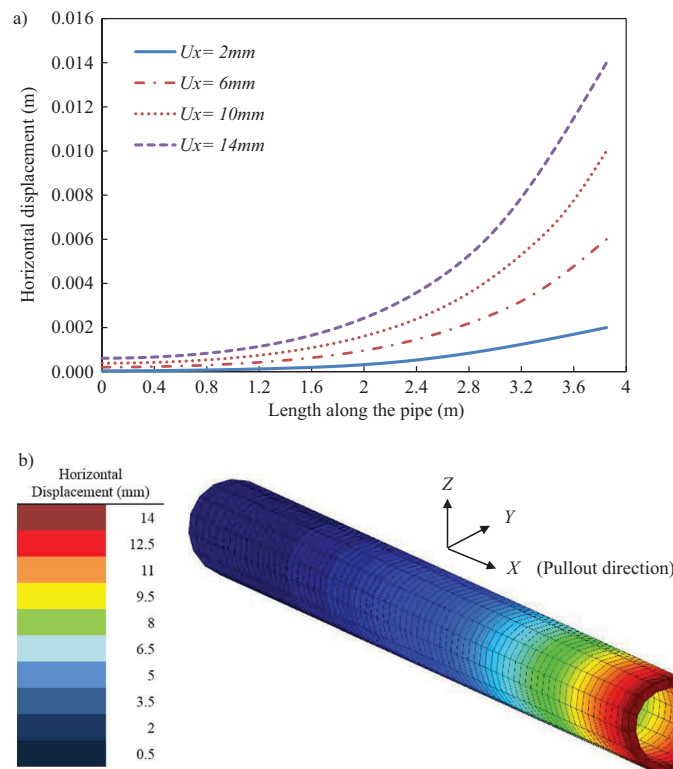


Figure 11. (a) Horizontal displacements along the pipe at different leading-end displacements; (b) distribution of horizontal displacements at $U_x = 14$ mm.

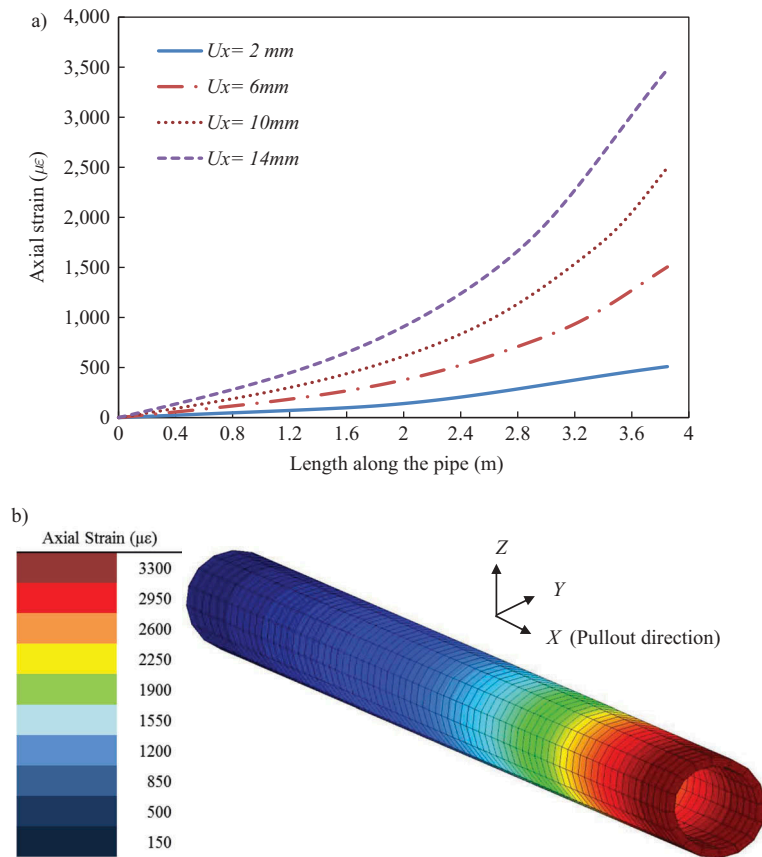


Figure 12. (a) Axial strain (ϵ_x) distribution in the pipe at different leading-end displacements; (b) Pipe axial strain at $U_x = 14\text{ mm}$.

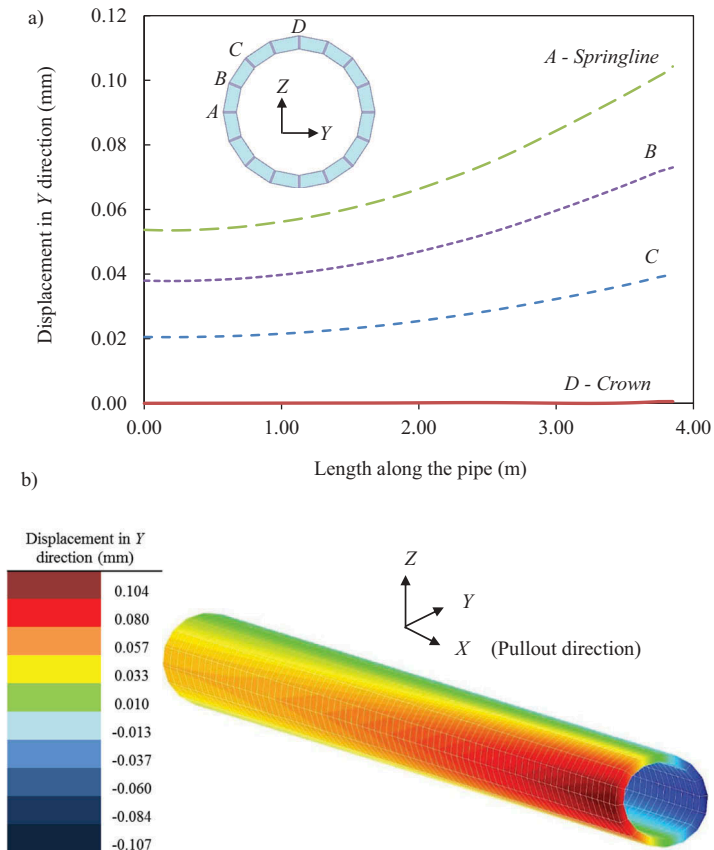


Figure 13. (a) Pipe displacements in the transverse direction for leading-end movement of 14 mm; (b) three-dimensional distribution of lateral deformations in the pipe structure.

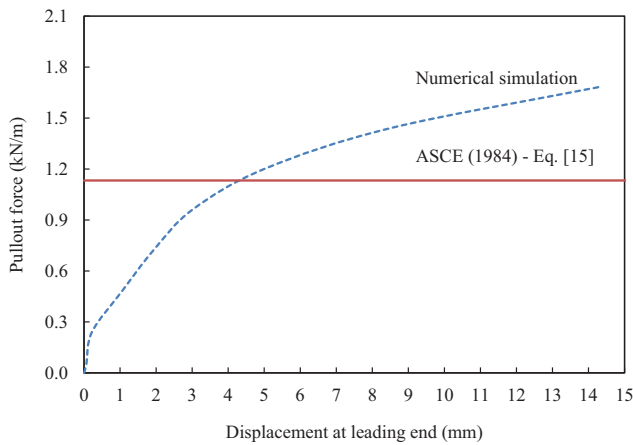


Figure 14. Comparison of the axial soil resistances (pull-out force) obtained using the numerical and closed form solutions.

pipe. As the pipe is pulled out, the particles near the front face start to move in the pull-out direction resulting in dilative response in the close vicinity of the pipe. This has led to an increase in the magnitude of the contact forces in zone A as shown in Figure 16b. These results allowed for better understanding of the interaction between PE pipe and the surrounding soil material under axial loading conditions.

5. Summary and conclusions

In this study, a finite-discrete element framework is employed to investigate the behaviour of a MDPE pipe buried in dense sand under axial loading condition. In this 3D analysis, soil

particles are modelled using discrete elements whereas the pipe structure is modelled using finite elements. Interface elements are introduced to transfer the forces between the discrete and finite element domains. Particles are generated following the grain size distribution of the Fraser River Sand used in the experiments. Input parameters required for the discrete elements are determined by calibrating the generated assembly using triaxial test results. The pull-out process is numerically simulated and the results are compared with experimental data as well as the available closed-form solution. Deformations and strains developing in the pipe as well as the response of the backfill material are investigated.

Most of the pipe deformation and strains developed near the loaded side and progressively decreased with distance towards the trailing end. For the investigated conditions, the pipe experienced significant elongation combined with a slight distortion in the pipe cross-section. This finding is in contrast with the assumption used in closed-form solutions that consider the pipe as a rigid element with uniform frictional resistance mobilized along the entire length of the pipe. This assumption can result in overestimating the soil frictional resistance for flexible pipes. In addition, dilation of the dense sand material during pull-out results in earth pressure that differs from the at-rest condition. This can be significant and may result in underestimating the axial soil resistance for flexible pipes buried in dense material.

Finally, the coupled FE-DE framework presented in this study has proven to be effective in studying the response of buried PE pipe subjected to axial ground movement. The pipe deformation and strain as well as the soil response can be captured using the proposed framework.

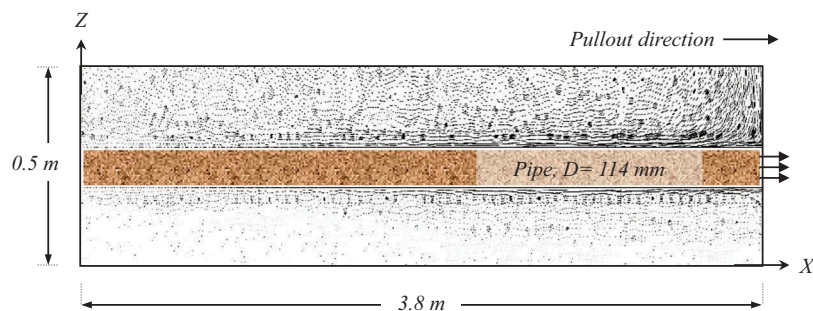


Figure 15. Displacement field in the soil domain at $U_x = 14$ mm.

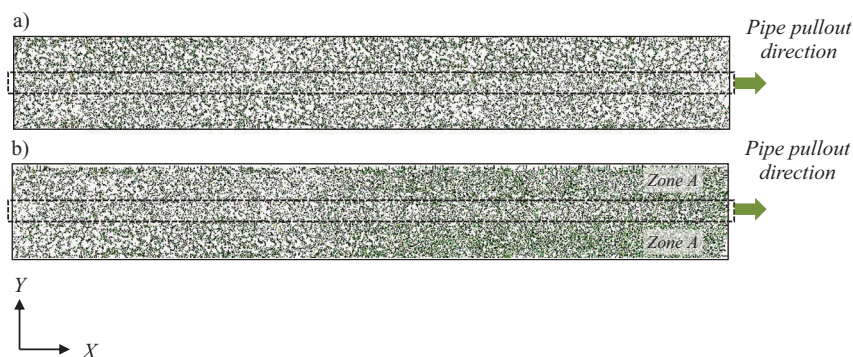


Figure 16. Top view showing the contact force network in the soil domain for: (a) initial condition (before pull-out); (b) for pull-out displacement of 14 mm.

Acknowledgements

This research is supported by the Natural Sciences and Engineering Research Council of Canada (NSERC). Financial support provided by McGill Engineering Doctoral Award (MEDA) to the first author is appreciated.

Disclosure statement

No potential conflict of interest was reported by the authors.

Funding

This research is supported by the Natural Sciences and Engineering Research Council of Canada (NSERC).

ORCID

Mohamed A. Meguid  <http://orcid.org/0000-0002-5559-194X>

References

- Ahmed, M., V. Tran, and M. A. Meguid. 2015. "On The Role Of Geogrid Reinforcement in Reducing Earth Pressure on Buried Pipes: Experimental and Numerical Investigations." *Soils and Foundations* 55 (3): 588–599. doi:10.1016/j.sandf.2015.04.010.
- ALA. 2001. Guideline for the Design of Buried Steel Pipe. American Lifeline Alliance (ALA), Accessed April 10 2018. www.americanlifelinealliance.org/Product_new3.htm
- Almahakeri, M., I. D. Moore, and A. Fam. 2016. "Study Of Longitudinal Bending in Buried Gfrp Pipes Subjected to Lateral Earth Movements." 8 (1): 04016012-1-04016012-12.
- Anderson, C. 2004. Soil–Pipeline Interaction of Polyethylene Natural Gas Pipelines in Sand. M.Sc. thesis, Department of Civil Engineering, University of British Columbia, Vancouver, B.C.
- ASCE. 1984. *Guidelines for the Seismic Design of Oil and Gas Pipeline Systems*. New York: Committee on Gas and Liquid Fuel Lifelines, American Society for Civil Engineering (ASCE).
- Bilgin, O., H. E. Stewart, and T. D. O'Rourke. 2007. "Thermal and Mechanical Properties of Polyethylene Pipes." *Journal of Materials in Civil Engineering* 19 (12): 1043–1052. doi:10.1061/(ASCE)0899-1561(2007)19:12(1043).
- Chen, C., G. R. McDowell, and N. H. Thom. 2012. "Discrete Element Modelling Of Cyclic Loads Of Geogrid-reinforced Ballast under Confined and Unconfined Conditions." *Geotextiles and Geomembranes* 35 (12): 76–86. doi:10.1016/j.geotexmem.2012.07.004.
- Cocchetti, G., C. Di Prisco, A. Galli, and R. Nova. 2009. "Soil–Pipeline Interaction along Unstable Slopes: A Coupled Three-Dimensional Approach. Part I: Theoretical Formulation." *Canadian Geotechnical Journal* 46 (11): 1289–1304. doi:10.1139/T09-028.
- Cui, L., and C. O'Sullivan. 2006. "Exploring the Macro-And Micro-Scale Response of an Idealized Granular Material in the Direct Shear Apparatus." *Geotechnique* 56 (7): 455–468. doi:10.1680/geot.2006.56.7.455.
- Daiyan, N., S. Kenny, R. Phillips, and R. Popescu. 2011. "Investigating Pipeline-Soil Interaction under Axial–Lateral Relative Movements in the Sand." *Canadian Geotechnical Journal* 48 (11): 1683–1695. doi:10.1139/t11-061.
- Dang, H. K., and M. A. Meguid. 2010. "Algorithm to Generate a Discrete Element Specimen with Predefined Properties." *International Journal of Geomechanics* 10 (2): 85–91. doi:10.1061/(ASCE)GM.1943-5622.0000028.
- Dang, H. K., and M. A. Meguid. 2013. "An Efficient Finite-Discrete Element Method for Quasi-Static Nonlinear Soil-Structure Interaction Problems." *International Journal for Numerical and Analytical Methods in Geomechanics* 37 (2): 130–149. doi:10.1002/nag.v37.2.
- Ding, X., L. Zhang, H. Zhu, and Q. Zhang. 2014. "Effect of Model Scale and Particle Size Distribution on PFC3D Simulation Results." *Rock Mechanics and Rock Engineering* 47: 2139–2156. doi:10.1007/s00603-013-0533-1.
- European Gas Pipeline Incident Data Group, 2015. Gas Pipeline Incidents. European Gas pipeline Incident Data Group (EGIG), Groningen, Netherlands. 9th EGIG Report 1970–2015, No. EGIG 05-R-0002.
- Fakhimi, A. 2009. "A Hybrid Discrete–Finite Element Model for Numerical Simulation of Geomaterials." *Computers and Geotechnics* 36 (3): 386–395. doi:10.1016/j.compgeo.2008.05.004.
- Guo, P. J., and D. F. E. Stolle. 2005. "Lateral Pipe-Soil Interaction in Sand with Reference to Scale Effect." *Journal of Geotechnical and Geoenvironmental Engineering*, ASCE 131 (3): 338–349. doi:10.1061/(ASCE)1090-0241(2005)131:3(338).
- Han, K., D. R. J. Owen, and D. Peric. 2002. "Combined Finite/Discrete Element and Explicit/Implicit Simulations of Peen Forming Process." *Engineering Computations* 19 (1): 92–118. doi:10.1108/02644400210413667.
- Hoeg, K. 1968. "Stresses against Underground Structural Cylinders." *Journal of Soil Mechanics and Foundations*. ASCE 94 (4): 833–858.
- Joshaghani, M. S., A. M. Raheem, and M. R. Mousavi. 2016. "Analytical Modeling of Large-Scale Testing of Axial Pipe-Soil Interaction in Ultra-Soft Soil." *American Journal of Civil Engineering and Architecture* 4 (3): 98–105.
- Karimian, H., 2006. Response of Buried Steel Pipelines Subjected to Longitudinal and Transverse Ground Movement. Ph.D. thesis, Department of Civil Engineering, The University of British Columbia, Vancouver, B.C.
- Konder, R. B. 1963. "Hyperbolic Stress-Strain Response: Cohesive Soils." *Journal of the Soil Mechanics and Foundations Division*, ASCE 89 (SM1): 115–143.
- Konuk, I., R. Hilips, S. Urley, and M. J. Paulin, 1999. Preliminary Ovalization Measurement of Buried Pipelines Subject to Lateral Bending. Submitted to 18th offshore mechanics and arctic engineering conference, St. John's, NF.
- Kozicki, J., and V. F. Donzé. 2008. "A New Open-Source Software Developed for Numerical Simulations Using Discrete Modeling Methods." *Computer Methods in Applied Mechanics and Engineering* 197: 49–50. doi:10.1016/j.cma.2008.05.023.
- Kunert, H. G., J. L. Otegui, and A. Marquez. 2012. "Nonlinear FEM Strategies for Modeling Pipe-Soil Interaction." *Engineering Failure Analysis* 24: 46–56. doi:10.1016/j.engfailanal.2012.03.008.
- Meidani, M., M. A. Meguid, and L. E. Chouinard. 2017. "Evaluation of Soil–Pipe Interaction under Relative Axial Ground Movement." *Journal of Pipeline Systems Engineering and Practice* 8 (4): 04017009. doi:10.1061/(ASCE)PS.1949-1204.0000269.
- Mohamedzein, Y. E., and M. Y. Al-Aghbari. 2016. "Experimental Study of the Performance of Plastic Pipes Buried in Dune Sand." *International Journal of Geotechnical Engineering* 10 (3): 236–245. doi:10.1080/19386362.2015.1124508.
- Naeini, S. A., E. Mahmoudi, M. M. Shojaedin, and M. Misaghian. 2016. "Mechanical Response of Buried High-Density Polyethylene Pipelines under Normal Fault Motions." *KSCE Journal of Civil Engineering* 20 (6): 2253–2261. doi:10.1007/s12205-015-0695-3.
- Ono, K., Y. Yokota, Y. Sawada, and T. Kawabata. 2018. "Lateral Force–Displacement Prediction for Buried Pipe under Different Effective Stress Condition." *International Journal of Geotechnical Engineering* 12 (4): 420–428.
- Phillips, R., A. Nobahar, and J. Zhou (2004). Combined Axial and Lateral Pipe-Soil Interaction Relationships. In Proceedings of the International Pipeline Conference (IPC2004), Calgary.
- Rahman, M. A., and H. Taniyama. 2015. "Analysis of A Buried Pipeline Subjected to Fault Displacement: A DEM and FEM Study." *Soil Dynamics and Earthquake Engineering* 71 (1): 49–62. doi:10.1016/j.soildyn.2015.01.011.
- Rizkalla, M., G. R. Simmonds, and J. T. Uptrove 1991. Field Longitudinal Restraint Tests, NPS 16 Nevis Lateral, Internal report, Nova Corporation of Alberta.
- Robert, D. J., K. Soga, T. D. O'Rourke, and T. Sakanoue. 2016. "Lateral Load-Displacement Behavior of Pipelines in Unsaturated Sands."

- Journal of Geotechnical and Geoenvironmental Engineering* 142 (11): 04016060. doi:10.1061/(ASCE)GT.1943-5606.0001504.
- Roy, K., B. Hawlader, S. Kenny, and I. Moore. 2016. "Finite Element Modeling of Lateral Pipeline–Soil Interactions in Dense Sand." *Canadian Geotechnical Journal* 53 (3): 490–504. doi:10.1139/cgj-2015-0171.
- Šmilauer, V. et al., ed. 2010. Yade Documentation, The Yade Project, 1st ed., Accessed March 1 2017. <http://yade-dem.org/doc/>.
- Tran, V. D. H., M. A. Meguid, and L. E. Chouinard. 2013. "A Finite-Discrete Element Framework for the 3D Modeling of Geogrid–Soil Interaction under Pullout Loading Conditions." *Geotextiles and Geomembranes* 37: 1–9. doi:10.1016/j.geotextmem.2013.01.003.
- Tran, V. D. H., M. A. Meguid, and L. E. Chouinard. 2014. "Discrete Element and Experimental Investigations Of The Earth Pressure Distribution on Cylindrical Shafts." *International Journal Of Geomechanics* : 80–91. doi: 14 doi:10.1061/(ASCE)GM.1943-5622.0000277.
- Trautmann, C. H., and T. D. O'Rourke, 1983. Behavior of Pipe with Dry Sand under Lateral and Uplift Loading, Geotechnical Engineering Report 83–7, Cornell University, Ithaca, N.Y.
- Villard, P. B., B. Chevalier, L. Hello, and G. Combe. 2009. "Coupling between Finite and Discrete Element Methods for the Modeling of Earth Structures Reinforced by Geosynthetic, Computers and Geotechnics, Vol." 36, No 5: 709–717.
- Weerasekara, L. 2007. Response of Buried Natural Gas Pipelines Subjected to Ground Movements. M.A.Sc. thesis, Department of Civil Engineering, University of British Columbia, Vancouver, B.C.
- Weerasekara, L., and D. Wijewickreme. 2008. "Mobilization of Soil Loads on Buried, Polyethylene Natural Gas Pipelines Subject to Relative Axial Displacements." *Canadian Geotechnical Journal* 45: 1237–1249. doi:10.1139/T08-043.
- Zhang, J., Z. Liang, and C. Han. 2016. "Mechanical Behavior Analysis of the Buried Steel Pipeline Crossing Landslide Area." *Journal of Pressure Vessel Technology* 138 (5): 051702. doi:10.1115/1.4032991.